

Photoluminescence from Chemically Exfoliated MoS₂

Goki Eda,^{*,†,‡,§} Hisato Yamaguchi,^{‡,§} Damien Voiry,[‡] Takeshi Fujita,^{§,||} Mingwei Chen,[§] and Manish Chhowalla[‡]

[†]Department of Materials, Imperial College London, Exhibition Road, London SW7 2AZ, U.K.

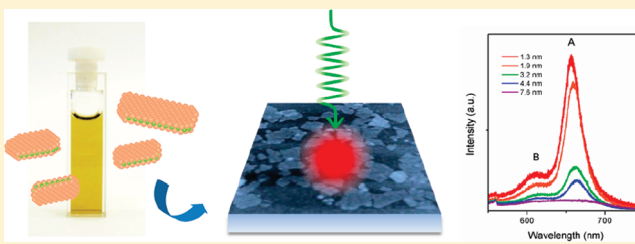
[‡]Materials Science and Engineering, Rutgers University, 607 Taylor Road, Piscataway, New Jersey 08854, United States

[§]WPI Advanced Institute for Materials Research, Tohoku University, Sendai 980-8577, Japan

^{||}JST, PRESTO, 4-1-8 Honcho Kawaguchi, Saitama 332-0012, Japan

 Supporting Information

ABSTRACT: A two-dimensional crystal of molybdenum disulfide (MoS₂) monolayer is a photoluminescent direct gap semiconductor in striking contrast to its bulk counterpart. Exfoliation of bulk MoS₂ via Li intercalation is an attractive route to large-scale synthesis of monolayer crystals. However, this method results in loss of pristine semiconducting properties of MoS₂ due to structural changes that occur during Li intercalation. Here, we report structural and electronic properties of chemically exfoliated MoS₂. The metastable metallic phase that emerges from Li intercalation was found to dominate the properties of as-exfoliated material, but mild annealing leads to gradual restoration of the semiconducting phase. Above an annealing temperature of 300 °C, chemically exfoliated MoS₂ exhibit prominent band gap photoluminescence, similar to mechanically exfoliated monolayers, indicating that their semiconducting properties are largely restored.



KEYWORDS: MoS₂, photoluminescence, exfoliation, phase transformation, dispersion

Atomically thin sheets of layered inorganic compounds such as metal chalcogenides and oxides represent an emerging class of materials with prospects for a range of applications.^{1–5} Layered transition-metal dichalcogenides (LTMDs) form a large family of materials with interesting properties that have been studied for decades.⁶ Crystals of LTMDs can be easily cleaved along the layer plane due to weak van der Waals forces between the layers similar to graphite. Individual monolayers of LTMDs can be isolated via micromechanical cleavage or the “Scotch tape method” used to obtain graphene from graphite.¹ The two-dimensional crystals of LTMDs are an inorganic analogue of graphene and represent the fundamental building blocks for other low-dimensional nanostructures such as inorganic nanotubes and fullerene.⁷

Molybdenum disulfide (MoS₂), a widely known LTMD, is a solid state lubricant and catalyst for hydrodesulfurization and hydrogen evolution.⁸ It is an indirect band gap semiconductor with an energy gap of ~1.2 eV in the bulk form⁹ and has also attracted interest as photovoltaic and photocatalytic materials.^{10,11} The band gap of MoS₂ increases with decreasing crystal thickness below 100 nm due to quantum confinement¹² and calculations predict it to reach 1.9 eV for a single monolayer.¹³ In addition to the increase in its size, the nature of the band gap also changes from indirect to direct when the thickness reaches a single monolayer.¹³ Recent success in isolating monolayers of MoS₂ has allowed the observation of strong photoluminescence that can be attributed to the direct gap electronic structure of monolayer MoS₂ (refs 14–16). The indirect-to-direct gap

transition results in giant enhancement (~10⁴) in photoluminescence quantum yield, highlighting the distinguishing feature of the monolayer compared to multilayer counterpart.¹⁵ Large in-plane carrier mobility of around 200–500 cm²/(V s) (ref 17) and robust mechanical properties of MoS₂ also make it an attractive material for flexible field-effect transistors (FETs).^{18,19} Recently Radisavljevic et al.²⁰ demonstrated high-performance FET fabricated using monolayer MoS₂ as the channel material with mobilities comparable to those of bulk crystals.

Exfoliation of MoS₂ into individual monolayers is a critical step toward making it optically active and implementing into novel devices. For practical applications, a scalable and controlled deposition technique is required.^{21,22} Coleman et al.²² recently proposed liquid-phase exfoliation of bulk MoS₂ powders in an appropriate organic solvent with aid of ultrasonication as a viable route to achieving this goal and demonstrated facile fabrication of bulk films and composites of the exfoliated material. This method yields thin sheets of MoS₂ with thicknesses of 3–12 nm, corresponding to 5–20 monolayers; however, monolayers were not observed. It has been previously shown by Morrison and co-workers²³ that Li-intercalated MoS₂ (Li_xMoS₂) can be exfoliated into monolayers via forced hydration, yielding a stable colloidal suspension. This method offers a versatile route

Received: June 2, 2011

Revised: October 10, 2011

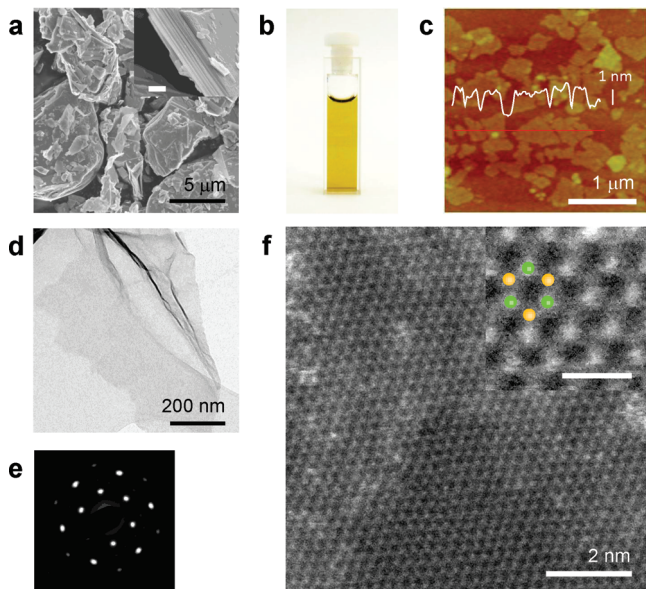


Figure 1. (a) Scanning electron microscopy image of MoS₂ powder. Inset shows higher magnification image of the layered structure. The scale bar is 400 nm. (b) Photograph of a typical chemically exfoliated MoS₂ suspension in water. (c) AFM image of individual exfoliated MoS₂ sheets after annealing at 300 °C. Height profile along the red line is overlaid on the image. The sample was prepared by filtering a small volume (~3 mL) of dilute MoS₂ suspension to minimize overlap between individual sheets. The resulting film was nonhomogeneous due to partial aggregation. Regions of the sample where the sheets were isolated were imaged for step height analysis. (d) TEM image of an as-deposited MoS₂ sheet on holey carbon grid. (e) SAED pattern from the MoS₂ sheet in (d) showing the hexagonal symmetry of the MoS₂ structure. (f) HAADF STEM image of monolayer MoS₂ annealed at 300 °C in Ar. Inset is a blow-up image showing individual Mo (green dot) and S (orange dot) atoms and their honeycomb arrangement. The scale bar is 0.5 nm. The white blur on the surface of the sheet is possibly due to carbon residues from the intercalation and exfoliation processes.

toward assembly of MoS₂ sheets into thin films,²⁴ formation of inclusion compounds,²⁵ and composites.²⁶ Facile solution-based deposition of thin films has also enabled their use as the hole transport layer in polymer light-emitting diodes.²⁷

While exfoliation of Li_xMoS₂ allows simple access to monolayer MoS₂, their physical properties have not been fully understood.²⁸ This is partly attributed to the phase changes that occur during Li intercalation and concomitant alteration of the pristine properties.²⁹ Specifically, Li intercalation results in loss of the semiconducting properties due to emergence of a metallic phase. In addition, the small size of the exfoliated flakes (typically <1 μm) and their tendency to aggregate upon deposition make study of the inherent monolayer properties challenging. Here, we show that the material consists of a mixture of two distinct phases and that their composition strongly determines their electronic properties. We demonstrate that the intercalation-induced phase transformation can be almost fully reversed via mild annealing such that the semiconducting properties of the pristine material are largely restored. The phase restoration is confirmed by the observation of band gap photoluminescence from ultrathin MoS₂ films.

A colloidal suspension of highly monodisperse monolayer MoS₂ sheets was prepared from commercial powder (Figure 1a) through Li intercalation and exfoliation followed by extensive

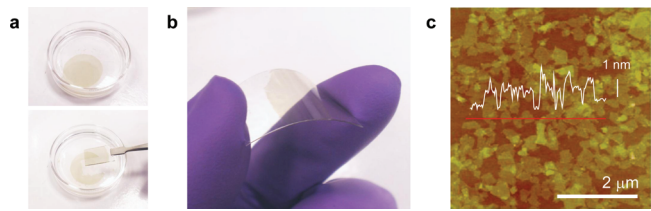


Figure 2. (a) Photograph of MoS₂ film floating on water (top panel) and deposited on glass (bottom panel). (b) Photograph of an as-deposited thin film of MoS₂ on flexible PET. The films in (a) and (b) are approximately 5 nm thick. (c) AFM image of an ultrathin film with an average thickness of 1.3 nm. The film consists of regions that are covered by monolayers and others that are slightly thicker due to overlap between individual sheets. Height profile along the red line is overlaid on the image.

purification (Figure 1b). A majority of the exfoliated MoS₂ sheets were found to be 300–800 nm in lateral dimensions and exhibited typical thickness of 1–1.2 nm (Figure 1c,d). The selected area electron diffraction (SAED) patterns indicate hexagonal symmetry of the atomic arrangement and that individual sheets consist of a single crystal domain (Figure 1e). The apparent thickness of the thin films shown in Figure 1c is larger than the 0.65–0.7 nm values reported for mechanically exfoliated MoS₂ monolayers.^{20,30} This discrepancy may be explained by surface corrugation due to distortions,³¹ the presence of adsorbed or trapped molecules (See Supporting Information for further atomic force microscopy (AFM) analysis). Absence of any sheets below the thickness values and no evidence of step edges on the nanosheets surface suggest that they consist of monolayers.

In order to unambiguously verify that a majority of exfoliated sheets are monolayers, we conducted high angle annular dark field scanning transmission electron microscopy (HAADF STEM) imaging. The STEM image shown in Figure 1f clearly reveals the honeycomb structure of MoS₂ where the Mo and S sites can be identified by differences in their contrast.^{22,32} Multilayers can be readily distinguished from monolayers in the STEM by examining the projected lattice images and the relative intensity of the lattice sites. For example, the two lattice sites are indistinguishable for commensurately stacked multilayer 2H-MoS₂ with stacking sequence of BcB AcA where the upper case and the lower case letters represent S and Mo layers, respectively.²² On the other hand, triangular lattice projection is expected for commensurately stacked multilayer 1T-MoS₂ with AbC AbC stacking sequence. Incommensurately stacked multilayers exhibit Moire patterns and can be readily distinguished from monolayers. Despite the possibility of local lattice distortions reported previously,³¹ our observations suggest that the honeycomb arrangement of the atoms extends over the entire sheet as indicated by the SAED patterns in Figure 1e.

Thin films of exfoliated MoS₂ sheets were fabricated by vacuum filtration of the suspension through a filter membrane with nanometer-sized pores.³³ The filter membrane with the MoS₂ film was slowly inserted into the water, allowing the film to delaminate from the membrane, which in turn resulted in a free-floating film on the water surface (Figure 2a). The intact floating MoS₂ film was captured by carefully scooping onto a substrate. Transfer was achieved on arbitrary substrates including glass and flexible PET (Figure 2b). The AFM image shown in Figure 2c demonstrates the remarkable uniformity of MoS₂ sheet coverage on Si/SiO₂ substrates. It should be noted that our thin film deposition method

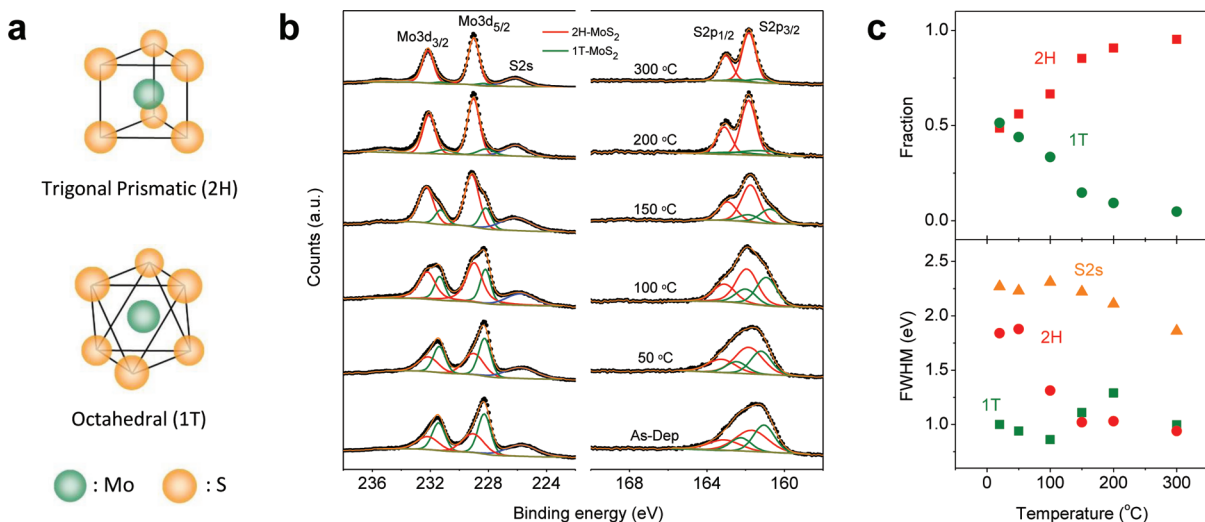


Figure 3. (a) Structure of 2H- and 1T-MoS₂. (b) XPS spectra showing Mo 3d, S 2s, and S 2p core level peak regions for samples annealed at various temperatures. The samples were measured on Pt foil and Pt 4f_{7/2} was taken as a reference. After Shirley background subtraction, the Mo 3d and S 2p peaks were deconvoluted to show the 2H and 1T contributions, represented by red and green plots, respectively. (c) Extracted relative fraction of 2H and 1T components (top) and the linewidths of S 2s and Mo 3d_{5/2} peaks as a function of annealing temperature (bottom). The Mo 3d_{5/2} peak linewidths are shown for the two phases. A similar trend was also observed for the S 2p peaks, but the data are not shown here for clarity.

allows extremely fine control over the film thickness ranging from near-monolayer up to tens of nanometers via adjustment of the filtration volume or the concentration of the suspensions used. The thickness of ~1 nm films reported here is distinctly thinner than those obtained previously by the spreading method,²⁴ which results in films thicker than 3 nm (ref 27). Our films exhibit some inhomogeneity, consisting of regions with slight variations in the number of layers as shown in Figure 2c.

Raman spectra of all samples showed the well-known in-plane E_{2g}¹ and out-of-plane A_{1g} peaks of 2H-MoS₂ both before and after annealing (See Supporting Information for details.) Frequencies of these Raman modes have been shown to indicate the number of layers in mechanically exfoliated MoS₂.³⁴ However, due to local variations in film thickness and the rotational stacking disorder, frequencies of these Raman modes do not allow direct determination of the number of layers in our samples. Instead, average film thicknesses have been calculated from AFM as discussed in the Supporting Information.

A thermodynamically stable form of MoS₂ is the trigonal prismatic (2H-MoS₂) phase where each molybdenum atom is prismatically coordinated by six surrounding sulfur atoms⁶ (Figure 3a). Upon Li intercalation, MoS₂ undergoes a first-order phase transition to a metastable phase where the coordination of Mo atoms becomes octahedral (1T-MoS₂)²⁹ (Figure 3a). The intriguing consequence of this phase transition is the dramatic change in the density of states which renders 1T-MoS₂ metallic.³⁵ The structure of chemically exfoliated MoS₂ sheets has been the subject of several studies²⁸ and is believed to be of 1T-type but with lattice distortions.³⁶ While annealing at moderate temperatures (~200 °C) is likely to cause transformation back to the initial 2H phase,³⁷ the extent of its restoration is not known. The phase transformation is also suggested to be triggered by removal of interlayer water in deposited films³⁸ and also progresses at lower temperatures over a period of weeks.³⁹ In this study, all experiments and measurements were conducted within 2 days from deposition in order to avoid aging effects.

Due to the differences in the symmetry elements in their structures, 2H and 1T phases can be differentiated by Raman analysis.³⁹ The as-deposited samples exhibit Raman peaks suggesting the presence of a 1T phase; however, due to its weak response, quantitative analysis of the phase composition was not possible (see Supporting Information). Instead we study the phase compositions by X-ray photoelectron spectroscopy (XPS). The Mo 3d, S 2s, and S 2p regions of the XPS spectra for samples annealed at various temperatures are shown in Figure 3b. The Mo 3d spectra consist of peaks at around 229 and 232 eV that correspond to Mo⁴⁺ 3d_{5/2} and Mo⁴⁺ 3d_{3/2} components of 2H-MoS₂, respectively. Deconvolution of these peaks reveals additional peaks that are shifted to lower binding energies by ~0.9 eV with respect to the position of the 2H-MoS₂ peaks. Similarly, in the S 2p region of the spectra, additional peaks are found besides the known doublet peaks of 2H-MoS₂, S 2p_{1/2}, and S 2p_{3/2}, which appear at 163 and 161.9 eV, respectively. The parallel shift of these additional peaks suggests that they arise from the 1T phase. Our observations are similar to those reported for single crystal MoS₂ progressively intercalated by Li where additional peaks appear due to formation of 1T phase.⁴⁰ The 1T peaks are gradually quenched after annealing above 100 °C. It is worth noting that absence of a prominent peak at around 236 eV, which corresponds to Mo⁶⁺ 3d_{5/2}, indicates that oxidation of Mo is minimal. Similarly, no peaks were observed between 168 and 170 eV, which indicates that sulfur atoms also remain unoxidized. Extracted phase compositions show that the as-deposited samples consist of nearly equal amounts of the two phases (Figure 3c). Increase of the 2H phase fraction is nearly linear with temperature up to about 150 °C and becomes gradual for higher temperatures. After annealing at temperatures above 200 °C, the material is predominantly in 2H phase, reaching 0.95 at 300 °C. It can also be noticed that the line width of 2H-MoS₂ peaks becomes progressively narrower with annealing above 150 °C, suggesting improved structural uniformity and relaxation of local strain (Figure 3c).

As-deposited films with thickness below 10 nm were semi-transparent and electrically conducting, but the conductivity

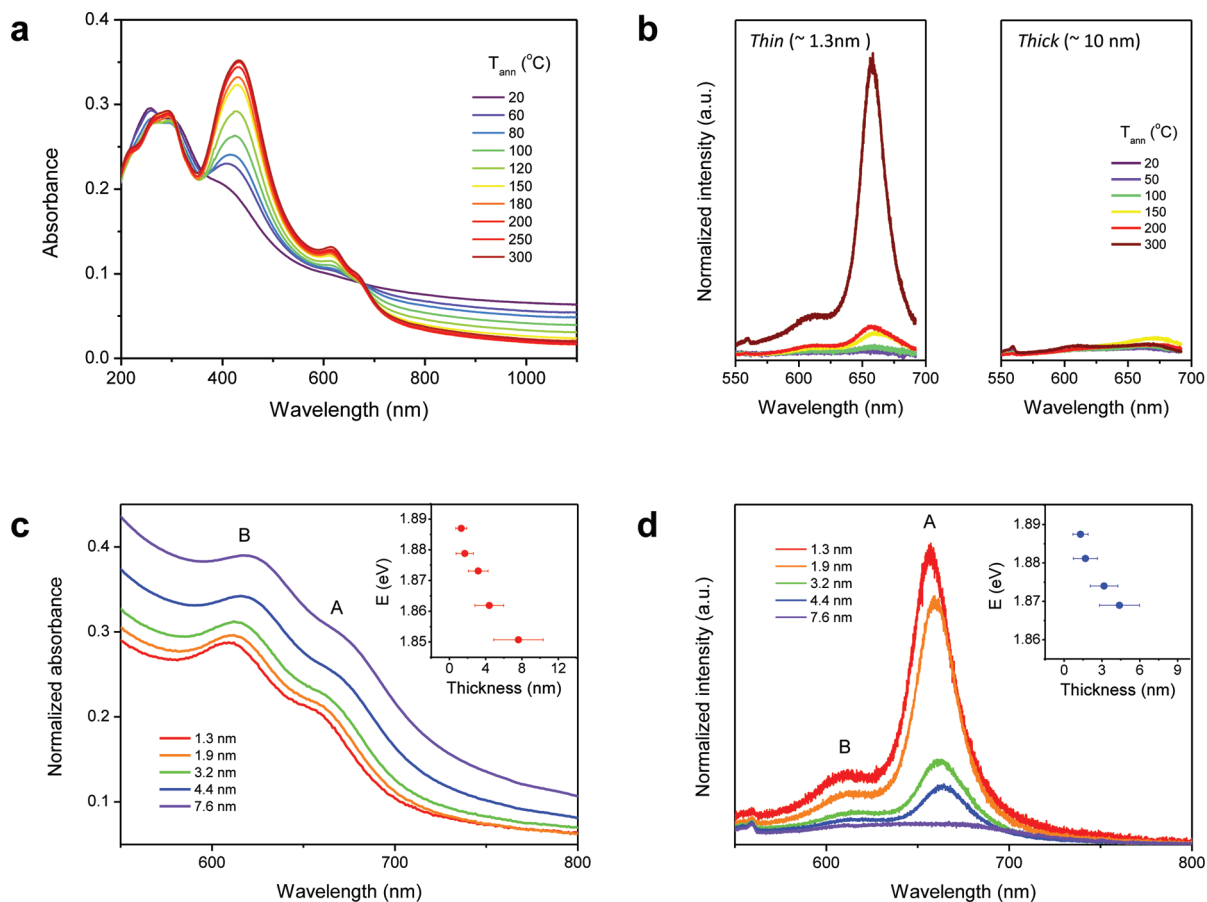


Figure 4. (a) Absorption and (b) photoluminescence spectra of MoS_2 thin films annealed at various temperatures. In (b), two sets of spectra for thin and thick samples are shown. Photoluminescence was measured with excitation wavelength at 514 nm. The spectra are normalized with the intensity of the A_{1g} Raman peaks. (c) Absorption and (d) photoluminescence spectra of MoS_2 thin films with average thicknesses ranging from 1.3 to 7.6 nm. The average film thickness and error bars were obtained from the height analysis of the AFM data (Supporting Information). Insets of (c) and (d) show energy of the A exciton peak as a function of average film thickness. The peak energies were extracted from the absorption and photoluminescence spectra in the main panel, respectively. No clear A exciton peak was identified in the emission spectrum of 7.6 nm film.

quickly dropped with annealing (Supporting Information). These films typically exhibited resistivity of $\sim 1 \Omega \cdot \text{cm}$ while values as large as $\sim 10^6 \Omega \cdot \text{cm}$ were observed after annealing at 300 °C. The unusually large resistivity of annealed films suggests non-negligible contributions from interflake resistance and residual defects that localize carriers. Nevertheless, significant increase in resistivity largely reflects the evolution of phase composition. We observed weak field modulated conductivity for annealed samples suggesting restoration of the semiconducting properties (Supporting Information).

Evolution of the mixed phase structure was further studied by measuring the absorption spectra of MoS_2 films as a function of progressive annealing (Figure 4a). As-deposited films exhibit no clear characteristic peaks of pristine 2H- MoS_2 except for the high energy excitonic features in the near-UV range (200–300 nm). With increasing annealing temperature, the characteristic MoS_2 excitonic features emerge and grow in intensity. Specifically, A and B excitonic peaks arising from the K point of the Brillouin zone were observed between 600 and 700 nm while convoluted C and D excitonic peaks appeared around 420 nm. Emergence of these features indicates restoration of 2H phase upon annealing. As compared to the pristine mechanically exfoliated monolayer, the exciton peaks are less resolved, suggesting the presence of residual structural disorder,

probably owing to remnant lattice distortion.³⁹ Gradually suppressed absorption in the near-IR region, which is below the band gap of 2H- MoS_2 , also suggests reduction of the metallic 1T phase component.

In order to evaluate the restored semiconducting phase, we investigated the photoluminescence properties of our samples. Monolayer of MoS_2 is a direct gap semiconductor where the lowest energy interband transition occurs at the K point of the Brillouin zone.¹³ Relaxation of excitons at the K point can result in emission of photons with energy of 1.9 eV (ref 15). Our as-deposited MoS_2 films do not exhibit photoluminescence, as expected from their partial metallic character. On the other hand, annealed films exhibit reproducible photoluminescence when their thickness is sufficiently low (< 5 nm). Figure 4b shows photoluminescence spectra of thin (~ 1.3 nm) and thick (~ 10 nm) films after annealing at different temperatures. For direct comparison, the spectra are normalized with A_{1g} Raman peak intensity. Gradual increase in the emission intensity with annealing temperature is observed for the thinner film while no emission is observed from the thick film even after annealing. The emission spectra for the thin film consist of one major peak and one minor peak at around 660 and 610 nm, respectively. These peaks, labeled as A and B, agree well with the energy of A and B excitons,

suggesting that they are from the direct band gap photoluminescence from the K point. The emission spectrum of our ~ 1.3 nm film is in good agreement with those reported by Mak et al.¹⁵ and Splendiani et al.¹¹ for mechanically exfoliated monolayer samples, indicating that the observed photoluminescence arises from the intrinsic electronic properties of monolayer MoS₂ and not from structural defects or chemical impurities. The emission intensity for our thinnest samples (~ 1.3 nm in average thickness) was comparable to that for mechanically exfoliated monolayers. (See Supporting Information for the comparison.) Defects with unsaturated Mo or S bonds which introduce midgap states are expected to be active nonradiative recombination centers for excitons.⁴¹ Our observations suggest that despite the possible residual structural disorder in our samples, density of such critical defects is sufficiently low.

Increase in film thickness was found to result in a slight red shift in both the absorption resonance and photoluminescence energy (Figure 4c,d). The shift is small (~ 20 meV) but consistent with the fact that direct gap is only weakly sensitive to the confinement effect due to the large electron and hole mass around the K point, changing by only 20 meV between mono- and bilayer MoS₂ (ref 15). Figure 4d shows that the thinnest samples exhibit the strongest photoluminescence while the emission intensity gradually decreases with increasing film thickness. The gradual quenching of photoluminescence with film thickness is in contrast to that in mechanically exfoliated MoS₂ where the quantum yield drops rapidly from monolayer to bilayer. Our observation may be explained by the fact that there may be monolayered regions within the multi-layered films. Alternatively, weak interlayer coupling between the restacked MoS₂ sheets due to rotational stacking disorder as suggested by Raman analysis could be responsible for the gradual decrease in PL. (See Supporting Information for details.)

Solution-based exfoliation of layered materials is a promising route for producing 2D crystals in large scale and realizing their unique properties in practical applications. We have demonstrated chemical exfoliation of MoS₂ to individual monolayers and deposition of ultrathin films that are up to several layers in thickness. Unlike chemically derived graphene,⁴² MoS₂ sheets remain chemically unmodified so that their fundamental electronic properties are largely preserved. Our films exhibit prominent band gap photoluminescence that is consistent with the behavior of mechanically exfoliated MoS₂, indicating that despite the chemical exfoliation, the MoS₂ sheets retain structural integrity with sufficiently low density of critical defects which may inhibit luminescence. The thickness-dependent electronic structure and the unique two-phase behavior of MoS₂ reveal unusual versatility of this material. For example, the properties of metallic and semitransparent 1T-MoS₂ represent new opportunities in the development of transparent conductors. These features of chemically exfoliated MoS₂ make them attractive for novel electronic and optoelectronic devices such as nonvolatile memory, solar cells, and light-emitting diodes which remain to be explored.

Method. Lithium intercalation was achieved by immersing 3 g of natural MoS₂ crystals (Sigma-Aldrich) in 3 mL of 1.6 M butyllithium solution in hexane (Sigma-Aldrich) for 2 days in a flask filled with argon gas. The Li_xMoS₂ was retrieved by filtration and washed with hexane (60 mL) to remove excess lithium and organic residues. Exfoliation was achieved immediately after this (within 30 min to avoid deintercalation) by ultrasonication of Li_xMoS₂ in water for 1 h. The mixture was centrifuged several

times to remove excess lithium in the form of LiOH and unexfoliated material. Thin films were prepared by filtering a diluted suspension (0.01–0.1 mg/mL) through a mixed cellulose ester membrane with 25 nm pores (Millipore). The film was delaminated as described in the main text on water surface for subsequent transfer onto a substrate. AFM data were obtained in Digital Instruments Nanoscope IV in tapping mode with standard cantilevers with spring constant of 40 N/m and tip curvature < 10 nm. Annealing was conducted on a hot plate in Ar-filled glovebox with low vapor and oxygen levels (~ 1 ppm). Samples were annealed at a desired temperature for 1 h. Raman and photoluminescence spectra were measured with an InVia Raman microscope (Renishaw) at excitation laser wavelength of 514 nm. Absorption spectra were collected for films deposited on quartz substrates in a PerkinElmer Lambda 25 UV-vis spectrometer. X-ray photoelectron spectroscopy (XPS) measurements were performed with a Thermo Scientific K-Alpha spectrometer. All spectra were taken using a Al K α microfocused monochromatized source (1486.6 eV) with a resolution of 0.6 eV. The spot size was 400 μ m and the operating pressure was 5×10^{-9} Pa. The MoS₂ films were measured on Pt foil, and Pt 4f_{7/2} was taken as reference at 70.98 eV. XPS measurements were made immediately after annealing. The TEM image and corresponding SAED in Figure 1 were taken in a JEOL 2000X at 200 kV. HAADF STEM imaging was performed using JEOL JEM-2100F TEM/STEM with double spherical aberration (Cs) correctors (CEOS GmbH, Heidelberg, Germany) to attain high contrast images with a point-to-point resolution of ~ 1.0 Å. Collecting angle was between 100 and 267 mrad. The lens aberrations were optimized by evaluating the Zemlin tableau of an amorphous carbon. The residual spherical aberration was almost zero (Cs = -0.8 ± 1.2 μ m with 95% certification). The acceleration voltage was set to 120 kV, which is the lowest voltage with effective Cs correctors in the system.

■ ASSOCIATED CONTENT

■ **Supporting Information.** Details on X-ray diffraction, thermal analysis, afm analysis and film thickness determination, transparent and conducting properties, Raman spectroscopy, and comparison with mechanically exfoliated sample. This material is available free of charge via the Internet at <http://pubs.acs.org>.

■ AUTHOR INFORMATION

Corresponding Author

*E-mail: g.eda@nus.edu.sg.

Present Addresses

[†]Department of Physics, National University of Singapore, 2 Science Drive 3, Singapore 117542.

Author Contributions

[#]These authors contributed equally to this work.

■ ACKNOWLEDGMENT

G.E. acknowledges the Royal Society for the Newton International Fellowship and financial support from the Centre for Advanced Structural Ceramics (CASC) at Imperial College London. G.E. also acknowledges Singapore National Research Foundation for partly funding the research under NRF RF. H.Y. acknowledges the Japan Society for the Promotion of Science (JSPS)

for financial support through Postdoctoral Fellowship for Research Abroad. M.C., H.Y., and D.V. acknowledge Donald H. Jacobs' Chair funding from Rutgers University. This research was partly supported by JST, PRESTO.

■ REFERENCES

- (1) Novoselov, K. S.; Jiang, D.; Schedin, F.; Booth, T. J.; Khotkevich, V. V.; Morozov, S. V.; Geim, A. K. *Proc. Natl. Acad. Sci. U.S.A.* **2005**, *102*, 10451.
- (2) Rao, C. N. R.; Nag, A. *Eur. J. Inorg. Chem.* **2010**, 4244.
- (3) Ma, R. Z.; Sasaki, T. *Adv. Mater.* **2010**, *22*, 5082.
- (4) Lee, C.; Li, Q. Y.; Kalb, W.; Liu, X. Z.; Berger, H.; Carpick, R. W.; Hone, J. *Science* **2010**, *328*, 76.
- (5) Cho, S.; Butch, N. P.; Paglione, J.; Fuhrer, M. S. *Nano Lett.* **2011**, *11*, 1925–1927.
- (6) Wilson, J. A.; Yoffe, A. D. *Adv. Phys.* **1969**, *18*, 193.
- (7) Tenne, R. *Nat. Nanotechnol.* **2006**, *1*, 103.
- (8) Furimsky, E. *Catal. Rev.* **1980**, *22*, 371.
- (9) Roxlo, C. B.; Chianelli, R. R.; Deckman, H. W.; Ruppert, A. F.; Wong, P. P. *J. Vac. Sci. Technol., A* **1987**, *5*, 555.
- (10) Tributsch, H. *Ber. Bunsen-Ges. Phys. Chem.* **1977**, *81*, 361.
- (11) Fortin, E.; Sears, W. M. *J. Phys. Chem. Solids* **1982**, *43*, 881.
- (12) Neville, R. A.; Evans, B. L. *Phys. Status Solidi B* **1976**, *73*, 597.
- (13) Li, T. S.; Galli, G. L. *J. Phys. Chem. C* **2007**, *111*, 16192.
- (14) Splendiani, A.; Sun, L.; Zhang, Y. B.; Li, T. S.; Kim, J.; Chim, C. Y.; Galli, G.; Wang, F. *Nano Lett.* **2010**, *10*, 1271.
- (15) Mak, K. F.; Lee, C.; Hone, J.; Shan, J.; Heinz, T. F. *Phys. Rev. Lett.* **2010**, *105*, 136805.
- (16) Korn, T.; Heydrich, S.; Hirmer, M.; Schmutzler, J.; Schüller, C. *Appl. Phys. Lett.* **2011**, *99*, 102109.
- (17) Fivaz, R.; Mooser, E. *Phys. Rev.* **1967**, *163*, 743.
- (18) Ayari, A.; Cobas, E.; Ogundadegbe, O.; Fuhrer, M. S. *J. Appl. Phys.* **2007**, *101*, 014507.
- (19) Podzorov, V.; Gershenson, M. E.; Kloc, C.; Zeis, R.; Bucher, E. *Appl. Phys. Lett.* **2004**, *84*, 3301.
- (20) Radisavljevic, B.; Radenovic, A.; Brivio, J.; Giacometti, V.; Kis, A. *Nat. Nanotechnol.* **2011**, *6*, 147.
- (21) Stankovich, S.; Dikin, D. A.; Dommett, G. H. B.; Kohlhaas, K. M.; Zimney, E. J.; Stach, E. A.; Piner, R. D.; Nguyen, S. T.; Ruoff, R. S. *Nature* **2006**, *442*, 282.
- (22) Coleman, J. N.; Lotya, M.; O'Neill, A.; Bergin, S. D.; King, P. J.; Khan, U.; Young, K.; Gaucher, A.; De, S.; Smith, R. J.; Shvets, I. V.; Arora, S. K.; Stanton, G.; Kim, H. Y.; Lee, K.; Kim, G. T.; Duesberg, G. S.; Hallam, T.; Boland, J. J.; Wang, J. J.; Donegan, J. F.; Grunlan, J. C.; Moriarty, G.; Shmeliov, A.; Nicholls, R. J.; Perkins, J. M.; Grieveson, E. M.; Theuwissen, K.; McComb, D. W.; Nellist, P. D.; Nicolosi, V. *Science* **2011**, *331*, 568.
- (23) Joensen, P.; Frindt, R. F.; Morrison, S. R. *Mater. Res. Bull.* **1986**, *21*, 457.
- (24) Divigalpitiya, W. M. R.; Morrison, S. R.; Frindt, R. F. *Thin Solid Films* **1990**, *186*, 177.
- (25) Divigalpitiya, W. M. R.; Frindt, R. F.; Morrison, S. R. *Science* **1989**, *246*, 369.
- (26) Kirmayer, S.; Aharon, E.; Dovgolevsky, E.; Kalina, M.; Frey, G. L. *Philos. Trans. R. Soc., A* **2007**, *365*, 1489.
- (27) Frey, G. L.; Reynolds, K. J.; Friend, R. H.; Cohen, H.; Feldman, Y. *J. Am. Chem. Soc.* **2003**, *125*, 5998.
- (28) Heising, J.; Kanatzidis, M. G. *J. Am. Chem. Soc.* **1999**, *121*, 638.
- (29) Py, M. A.; Haering, R. R. *Can. J. Phys.* **1983**, *61*, 76.
- (30) Ghatak, S.; Pal, A. N.; Ghosh, A. *ACS Nano* **2011**, *5*, 7707–7712.
- (31) Yang, D.; Sandoval, S. J.; Divigalpitiya, W. M. R.; Irwin, J. C.; Frindt, R. F. *Phys. Rev. B* **1991**, *43*, 12053.
- (32) Hansen, L. P.; Ramasse, Q. M.; Kisielowski, C.; Brorson, M.; Johnson, E.; Topsøe, H.; Helveg, S. *Angew. Chem., Int. Ed.* **2011**, *50*, 10153–10156.
- (33) Eda, G.; Fanchini, G.; Chhowalla, M. *Nat. Nanotechnol.* **2008**, *3*, 270.
- (34) Lee, C.; Yan, H.; Brus, L. E.; Heinz, T. F.; Hone, J.; Ryu, S. *ACS Nano* **2010**, *4*, 2695.
- (35) Mattheis, Lf *Phys. Rev. B* **1973**, *8*, 3719.
- (36) Qin, X. R.; Yang, D.; Frindt, R. F.; Irwin, J. C. *Phys. Rev. B* **1991**, *44*, 3490.
- (37) Wypych, F.; Schollhorn, R. *J. Chem. Soc., Chem. Comm.* **1992**, 1386.
- (38) Qin, X. R.; Yang, D.; Frindt, R. F.; Irwin, J. C. *Ultramicroscopy* **1992**, *44*–42, 630.
- (39) Sandoval, S. J.; Yang, D.; Frindt, R. F.; Irwin, J. C. *Phys. Rev. B* **1991**, *44*, 3955.
- (40) Papageorgopoulos, C. A.; Jaegermann, W. *Surf. Sci.* **1995**, *338*, 83.
- (41) Kam, K. K.; Parkinson, B. A. *J. Phys. Chem.* **1982**, *86*, 463.
- (42) Park, S.; Ruoff, R. S. *Nat. Nanotechnol.* **2009**, *4*, 217.